Separating emitted dust from the total suspension in airflow based on the characteristics of PM10 vertical concentration profiles on a Gobi surface in northwestern China

ZHANG Chunlai[1], WANG Xuesong[1,2*], CEN Songbo[1], ZHENG Zhongquan Charlie[3], WANG Zhenting[4]

[1] State Key Laboratory of Earth Surface Processes and Resource Ecology, MOE Engineering Research Center of Desertification and Blown-sand Control, Faculty of Geographical Science, Beijing Normal University, Beijing 100875, China;
[2] School of Environment, Beijing Normal University, Beijing 100875, China;
[3] Aerospace Engineering Department, University of Kansas, Lawrence, KS 66045-7621, USA;
[4] Northwest Institute of Eco-Environment and Resources, Chinese Academy of Sciences, Lanzhou 730000, China

Abstract: During aeolian processes, the two most critical factors related to dust emissions are soil particle and aggregate saltation, which greatly affect the vertical profiles of near-surface dust concentrations. In this study, we measured PM10 concentrations at four different heights (0.10, 0.50, 1.00 and 2.00 m) with and without continuous and simultaneous aeolian saltation processes on a Gobi surface in northwestern China from 31 March to 10 April, 2017. We found that the vertical concentration profiles of suspended PM10 matched the log-law model well when there was no aeolian saltation. For the erosion process with saltation, we divided the vertical concentration profiles of PM10 into the saltation-affected layer and the airflow-transport layer according to two different dust sources (i.e., locally emitted PM10 and upwind transported PM10). The transition height between the saltation-affected layer and the airflow-transport layer was not fixed and varied with saltation intensity. From this new perspective, we calculated the airflow-transport layer and the dust emission rate at different times during a wind erosion event occurred on 5 April 2017. We found that dust emissions during wind erosion are primarily controlled by saltation intensity, contributing little to PM10 concentrations above the ground surface compared to PM10 concentrations transported from upwind directions. As erosion progresses, the surface supply of erodible grains is the most crucial factor for saltation intensity. When there was a sufficient amount of erodible grains, there was a significant correlation among the friction velocity, saltation intensity and dust emission rate. However, when supply is limited by factors such as surface renewal or an increase in soil moisture, the friction velocity will not necessarily correlate with the other two factors. Therefore, for the Gobi surface, compared to limiting dust emissions from upwind directions, restricting the transport of suspended dust in its path is by far a more efficient and realistic option for small areas that are often exposed to dust storms. This study provides some theoretical basis for correctly estimating PM10 concentrations in the Gobi areas.

Keywords: PM10; vertical concentration profiles; dust emission rate; saltation intensity; suspensions; Gobi surface

Citation: ZHANG Chunlai, WANG Xuesong, CEN Songbo, ZHENG Zhongquan Charlie, WANG Zhenting. 2022. Separating emitted dust from the total suspension in airflow based on the characteristics of PM10 vertical concentration profiles on a Gobi surface in northwestern China. Journal of Arid Land, 14(6): 589–603. https://doi.org/10.1007/s40333-022-0066-0

*Corresponding author: WANG Xuesong (Email: xswang@bnu.edu.cn)
Received 2022-02-11; revised 2022-05-13; accepted 2022-05-16

1 Introduction

The upward ejection of soil particles and their horizontal transport with airflow are two distinct subprocesses of the overall aeolian process (Dong et al., 2010; Shao et al., 2011; Zhang et al., 2018). Large particles are transported short distances during a single saltation or "creep" (Pye, 2009). Thus, the net surface upward sand flux is zero in steady state saltation. For small dust particles (e.g., PM10 particles), the net upward dust flux is approximately equal to the dust emission flux due to the long-term and long-distance transport associated with dust suspension (Gillette and Walker, 1977; Zender et al., 2003). Therefore, suspension above the ground surface during an erosion event is comprised of locally emitted dust and upwind transported dust. In other words, local emitted dust is only part of the suspension measured in local airflow.

There are no technological means thus far that can separate emitted dust from aeolian suspension for the purpose of directly studying dust emissions during aeolian processes. Currently, field studies on dust emissions and transport use two main methods. The first is the use of passive traps to collect aeolian horizontal mass from which to obtain the amount of suspension transport by separating dust from the total mass collected (Fryrear and Saleh, 1993; Leys and Mctainsh, 1996; Hagen et al., 2010; Wang et al., 2019). The second is the use of active aerosol monitors (e.g., TSI DustTrak) from which to monitor suspension concentrations in airflow (Nickling and Gillies, 1993; Gillies and Berkofsky, 2004; Zobeck and Pelt, 2006; Wagenbrenner et al., 2013; Wang et al., 2021). Compared to aerosol monitoring, the measurement accuracy of the traditional trap method is poor; namely, the collection efficiency is low, and there exists a disparity in collection efficiency between sand and suspended materials. Moreover, the aerosol monitoring method can provide more reliable data continuously and automatically, with less human disturbance on suspension transport under aeolian sand flow conditions (Zobeck and Pelt, 2006). However, neither method can offer a good solution to directly correlate dust emissions to measurements on the horizontal suspension transport. During field observations, flux-concentration relationships are typically used to indirectly reflect dust emissions (Nickling and Gillies, 1993; López, 1998; Zobeck and Pelt, 2006; Wagenbrenner et al., 2013; Wang and Zhang, 2021). Studies have shown that there is a correlation among vertical dust flux, horizontal suspension flux and dust emission flux, but this correlation remains unclear (Bagnold, 1941; Gillette et al., 1997; Whicker et al., 2014; Shao et al., 2020).

Based on aeolian-driven horizontal masses at various heights above the ground surface, Fryrear and Saleh (1993) investigated saltation and suspension using mathematical models. They hypothesized that the intersection was in fact the transition height between the saltation layer and the suspension layer, where the transport mode alters from saltation to suspension. However, dust particles can also be suspended in the saltation layer. Moreover, soil particles with diameters less than 20 μm are typically adsorbed into large particles or aggregates by electrostatic forces, making it more difficult to be directly lifted by airflow. Such particles are mainly emitted by saltation bombardment and suspended in airflow (Hinds, 1999). All such particles can significantly change the vertical profile of near-surface suspension concentration during wind erosion. Therefore, changes in suspension concentrations in the saltation layer cannot be ignored, and the vertical profile model should therefore be studied in a piecewise manner, by adding parameters to express changes in wind conditions and saltation intensity.

Previous studies on the vertical concentration profiles of suspensions have achieved some advances. For suspended particulate matter, if the ratio of the particle settling velocity (u_p) to the friction velocity (u_*) is less than 0.100, the particles move in a near-gaseous manner (Gillette, 1974; Kjelgaard et al., 2004). A threshold friction velocity (u_{*pt}) that allows suspended PM10 to move with airflow must therefore exist (Bagnold, 1941). Shao (2008) estimated a settling velocity of u_p to 10 μm particles at 0.008 m/s and then calculated the u_{*pt} for particles at approximately 0.080 m/s. When $u_*<u_{*pt}$, the vertical concentration is irregularly distributed. When $u_*>u_{*pt}$, the vertical concentration profile of suspensions is regular and closely related to atmospheric properties (e.g., wind speed, turbulent diffusion, etc.). The vertical concentration profile of

suspensions is an idealized mathematical expression that describes the profile under this condition. By theoretically analyzing the solution of the turbulent diffusion equation under conditions of equilibrium, the form of the concentration profiles that is predicted with respect to suspension has effectuated two expressions: the power-law profile and the logarithmic profile (Prandtl, 1953; Anderson and Hallet, 1986). The power-law profile is used to describe the vertical concentration profile of suspensions above surfaces that actively emit snow and mineral dust (Budd, 1965; Nickling and Gillies, 1993; Shao and Lu, 2000). However, Kind (1992) concluded that experimental data derived from the power-law profile for blowing snow experiments is based on erroneous boundary conditions at the surface of the particle bed, and the logarithmic profile can therefore more accurately describe the vertical concentration profiles of suspensions. Gillies and Berkofsky (2004) supported this conclusion using continuous observations of the vertical concentration profiles of suspensions outside the saltation-affected layer. Both the power-law and log-law models come from the same steady-state, i.e., horizontally homogeneous solution of particle transport (with the turbulent diffusion approximation), but the power-law model is the solution in the limit of zero net flux (larger dust particles), whereas the log-law model is the solution in the limit of zero settling (smaller dust particles) (e.g., Freire et al., 2016; Zhang et al., 2018).

In this study, we conducted a 12-d field observation of wind speed, saltation and PM10 concentrations at various heights on a Gobi surface. We discussed the expressions used for near-surface PM10 vertical concentration profiles with and without saltation and utilized the concentration transition height (TSA) between the saltation-affected layer and airflow-transport layer to determine regular patterns in dynamic dust emissions with a decrease in soil erodibility on the Gobi surface as wind erosion progresses. In addition, based on the relationship between the PM10 vertical concentration profiles, u_* and saltation intensity, we proposed a mathematical method from a new perspective to separate dust emitted from local and aeolian suspensions transported from an upwind direction in the saltation-affected layer during aeolian processes. Finally, we further discussed the transition between horizontal suspension flux and dust emission flux as well as the changes in their proportions during aeolian processes.

2 Materials and methods

2.1 Experimental site

Field observations were conducted on a flat and bare area of the Gobi desert within the Dunhuang City, Gansu Province, northwestern China (39°46′N; 94°24′E), from 31 March to 10 April, 2017. Dispersed particle size analysis measured using a vibrating screen machine and a Malvern Mastersizer laser diffractometer (Malvern Instruments, Malvern, UK) showed that the average particle size of sediment at the 0–1 cm soil layer was approximately 708 μm, and the proportion of particles finer than 10 μm in diameter was approximately 5.5%. Gravel covers 30.0%–40.0% of the total land in the study area, mainly ranging from 2 to 6 cm in diameter. The climate is continental arid with the annual mean temperature of 3.5°C, the mean annual precipitation of 120 mm and the annual mean wind speed of 2.700 m/s. The dominant wind direction in this region is northwest, and strong wind events occur frequently in spring. The recorded maximum instantaneous wind speed reached up to 26.000 m/s at a height of 10.00 m (Qiu et al., 2001).

The study area was slightly artificially disturbed. After removing weeds from the surface, we used half full petrol tanks filled with water to flatten the original surface; this was done by rolling the tanks in a backward and forward direction. The square study site with an area of 1 hm^2 (100 m×100 m) devoid of weeds and flattened through rolling was maintained this way for the whole duration of the study.

2.2 Physical background of the dust concentration profiles

In this study, we assumed horizontally homogeneous and steady-state conditions, a logarithmic mean horizontal wind, and zero mean vertical wind to simplify the problem and to make it

tractable. Under these conditions, particle concentration will not be impacted by horizontal advection (because everything is homogeneous), and the two physical processes that will impact dust concentration are vertical turbulent transport and gravitational settling. If the particle is too small, settling can be neglected, as the dust behaves as a passive scalar. The governing transport equation of dust can be expressed as:

$$w_s \frac{\partial c}{\partial z} - \frac{\partial \overline{w'c'}}{\partial z} = 0, \tag{1}$$

where w_s (m/s) is the settling velocity; c (mg/m^3) is the mean dust concentration; z (m) is the height above the ground surface; and w' (m/s) and c' (mg/m^3) are the fluctuations of vertical velocity and concentration (molecular diffusion was neglected), respectively. The model in the study of Kind (1992) can be used to calculate the mean particle concentration as a function of height. If $\overline{w'c'} = -K\partial c / \partial z$ (eddy diffusivity model) is used, the diffusivity K expressed as K=kzu_* (where k is the von Kármán constant (k=0.4) from the law-of-the-wall is defined, and both of them are integrated in the vertical direction. The following power-law equation can be obtained when there is no net flux at the surface:

$$\frac{c}{c_r} = \left(\frac{z}{z_r}\right)^{-w_s/\mathrm{k}u_*}, \tag{2}$$

where c_r (mg/m^3) is the dust concentration at reference height z_r (m); and u_* (m/s) is the friction velocity. If there is no settling velocity and net flux, then a constant profile can be obtained ($c(z)$=c_r, where $c(z)$ (mg/m^3) is the particle concentration at height z). When we assumed that we have no settling velocity but a positive net flux (Φ, mg/(m•s)), then the log-law profile can be expressed as follows:

$$\frac{c}{c_r} = 1 - \frac{\Phi}{\mathrm{k}u_* c_r}\left(\frac{z}{z_r}\right). \tag{3}$$

2.3 Instrumentation and data analysis

During the field observation period, a mast with nine rotating-cup anemometers, a mast with four sets of aerosol monitoring devices, and a set of automatic weighing sand traps were installed in a row in an orientation perpendicular to the dominant wind direction (Fig. 1).

The vertical profile of wind speed was monitored using rotating-cup anemometers (010C, Metone Inc., Washington, USA) installed at heights of 0.05, 0.10, 0.20, 0.30, 0.50, 0.75, 1.00, 2.00 and 3.00 m above the ground surface (Fig. 1a). All anemometers were calibrated in a wind tunnel at the State Key Laboratory of Earth Surface Processes and Resource Ecology, Beijing Normal University, Beijing, China. These anemometers recorded the mean wind speed at 30 s intervals using a data logger with the resolution of 0.100 m/s and measuring range of 0.300–30.000 m/s. In this study, only wind speed data that were relatively constant within 10 min (the ratio of the standard deviation to the mean wind speed was less than 0.150) were utilized. Using the least-square regression of the logarithmic law (Eq. 4) of a typical turbulent atmospheric boundary layer to the measured vertical profile of wind speed, we calculated the u_* and the aerodynamic roughness length (z_0; m) at an interval of 1 min.

$$u(z) = \frac{u_*}{\mathrm{k}} \ln\left(\frac{z}{z_0}\right), \tag{4}$$

where $u(z)$ (m/s) is the wind speed at height z.

We measured PM10 concentrations (mg/m^3) at heights of 0.10, 0.50, 1.00 and 2.00 m above the ground surface using four aerosol monitors (TSI DustTrak 8530, TSI Inc., Shoreview, Minnesota, USA) (Fig. 1b). Aerosol monitors can display and record real-time aerosol readings and have been successfully used to measure suspension concentrations during sandstorms (Gillies and Berkofsky, 2004; Macpherson et al., 2008; Sharratt and Pi, 2018; Wang and Zhang, 2021). The monitors had a resolution of 0.001 mg/m^3, an operating range from 0.001 to 400.000 mg/m^3 and

an overall efficiency between 60.0% and 95.0% (Houser and Nickling, 2001; Gillies and Berkofsky, 2004). Four aerosol monitors were placed 2.00 m downwind of the mast to reduce measurement interference. Each aerosol monitor was connected to a rubber pipe whose orifice was directed straight upward, then fixed on the mast at the given height. During the observation period, suspended PM10 particles in the air were sucked into the aerosol monitors via the rubber pipe, and the monitors could record the mean PM10 concentration every 5 s. If the field area is very small and the soil texture has relatively high homogeneity, namely, areas devoid of heterogeneous dust sources, the horizontal suspension flux at various heights may be determined by simply measuring the vertical profile of suspension concentration and then multiplying the results by wind speed (Zobeck and Pelt, 2006). Accordingly, the horizontal suspension flux (E; mg/(m^2•s)) at height z, the horizontal suspension transport rate (q_d; mg/(m•s)) and the horizontal suspension transport amount (Q_d; mg/m) below a given height (h; m) above the ground surface during a specific time period were calculated using the following equations:

$$E(z) = c(z) \times u(z), \tag{5}$$

$$q_d = \int_{z_0}^{h} E \mathrm{d}z, \tag{6}$$

$$Q_d = \int_{t_1}^{t_2} q_d \mathrm{d}t, \tag{7}$$

where the aerodynamic roughness length z_0 is 10^{-4} m in the present study; t_1 (min) and t_2 (min) are the starting and ending observation times, respectively; and t (min) is the observation period.

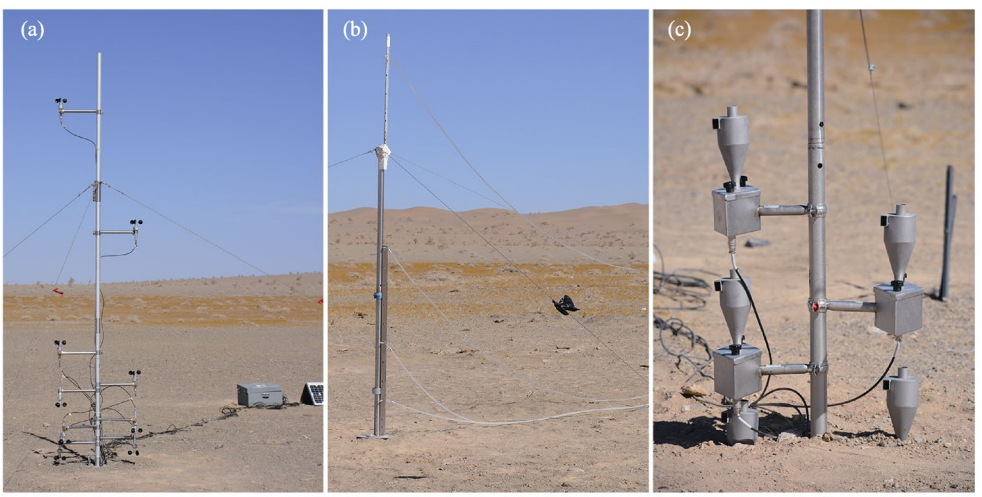

Fig. 1 Layout of the study site and the used instruments. (a), rotating-cup anemometers; (b), aerosol monitors; (c), automatic weighing sand traps.

The dynamic changes in the saltation mass were measured using a set of automatic weighing sand traps every 1 s (Fig. 1c). In this study, although the sand trap has five inlets at different heights, the sand flux (kg/(m^2•min)) measured by the lowest inlet at 0.05 m height (Q_z=0.05 m) was only used to reflect the saltation intensity. This was because the mass of the collected sand particles in other sand trap inlets was too small to weigh, which cannot reflect the dynamic changes.

Under low wind speeds (i.e., wind speed at 2.00 m height above the ground surface, $u_{2.00\,\mathrm{m}}$<2.000 m/s), owing to the instability of near-surface airflow, the vertical profile of wind speed was irregular. Moreover, the threshold wind speed at 2.00 m height above the ground surface, which makes suspended PM10 particles moving in a near-gaseous manner, was also approximately 2.000 m/s, as calculated by Equation 4 with u_*=u_{*pt} of PM10 (approximately 0.080 m/s) and the z_0 value of 10^{-4} m. Therefore, we only analyzed observation data under the condition that $u_{2.00\,\mathrm{m}}$ was

greater than 2.000 m/s and wind speed is relatively constant (i.e., time period was within 10 min and the ratio of standard deviation to the mean wind speed was less than 0.150). After filtering the data, we obtained effective 20 h data on suspension concentration observations in the study site, including one wind erosion event (14:08–18:08 (LST)) on 5 April 2017.

All of the fitting analyses and graphs were conducted using Origin 2016 software.

3 Results

3.1 Vertical profile of PM10 concentrations without saltation

Using the PM10 concentration data from four different observation heights (0.10, 0.50, 1.00 and 2.00 m) under wind speeds less than the threshold velocity of sand movement (i.e., under approximately 2.000 m/s), we evaluated the applicability of the vertical profile models proposed by Prandtl (1953) and Kind (1992) in the study area. We used 10 min average PM10 concentrations in this study. To compare the vertical concentration profiles of PM10 at different time periods, we normalized the absolute PM10 concentration data and measurement heights to a reference height measurement (0.10 m). Least-square regression was used to fit both the power and logarithmic regression models to the data (Fig. 2).

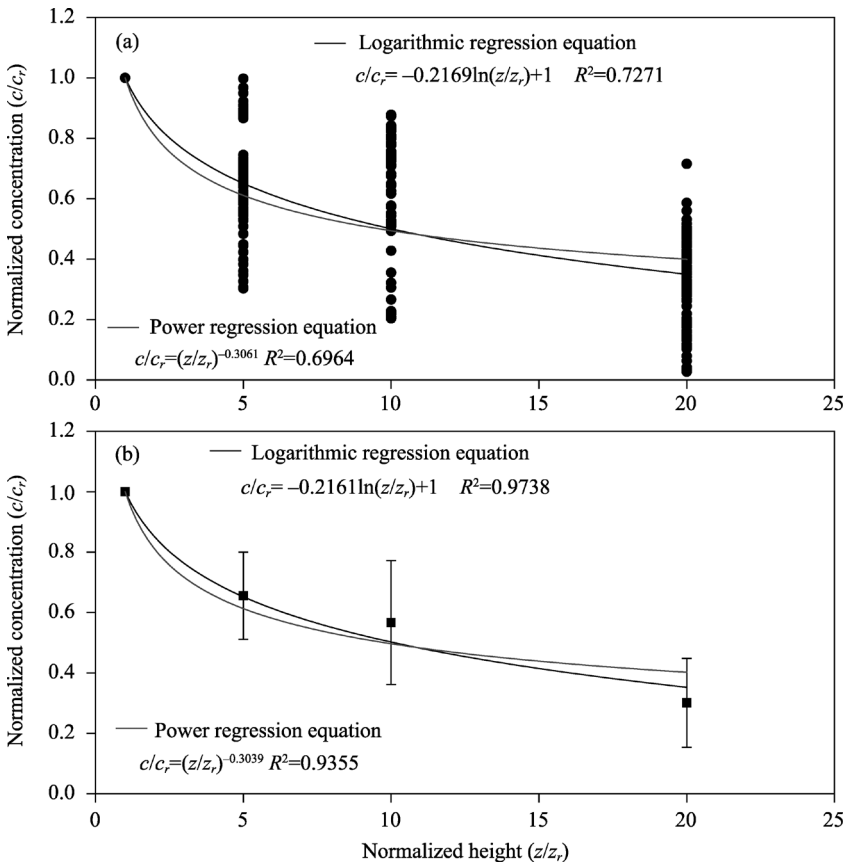

Fig. 2 Observed relationship between normalized concentration (c/c_r) and normalized height (z/z_r). (a), 10 min average data for 20 h; (b), the overall average data with error bars. c is the mean PM10 concentration at height z, and c_r is the PM10 concentration at reference height z_r. Regression equations that fit both the power and logarithmic regression models are shown.

It is obvious that the log-law profile model was more suitable for expressing the vertical concentration profile of PM10. This finding is consistent with results from previous theoretical derivation studies and field experiments (e.g., Kind, 1992; Gillies and Berkofsky, 2004). The

vertical concentration profile of PM10 can be expressed as follows:

$$\frac{c}{c_r} = a \ln\left(\frac{z}{z_r}\right) + 1, \tag{8}$$

where a is the regression coefficient, which can be expressed as: $a = -(\Phi/k u_* c_r)$ following Equation 3. According to Equation 3 and by setting z_r=1.00 m, we further deformed Equation 9 as follows:

$$c(z) = b \ln(z) + c(1), \tag{9}$$

where $c(1)$ (mg/m^3) is the PM10 concentration at a height of 1.00 m; and b is the regression coefficient, which can be expressed as: $b = -(\Phi/k u_*)$. If $u_{*pt} < u_* < u_{*t}$ (where u_{*t} (m/s) is the threshold friction velocity of sand movement), we can use Equation 9 to describe the vertical concentration profiles of PM10 on a bare and flat surface.

When the wind speed was less than the u_{*t}, almost no dust emissions resulting from saltation occurred. Although the convective dust might occur due to atmospheric instability under weak wind speed conditions, it was expected that the convective dust should be too small to be ignored since fine particles on the Gobi surface were between the coarse particles and protected by the coarse particles so that it was difficult to lift by weak wind. Suspensions above the ground surface were thus considered to be all transported from the upwind direction. At this point, the vertical concentration profiles of suspensions were closely associated with upwind conditions. Although the absolute suspension concentration is difficult to predict, the gradient of the vertical concentration profile can be predicted by its relationship with the u_*. According to Equation 9, b is clearly a function of the u_*. Here, we illustrated the relationship between b and u_* (Fig. 3), where b was obtained by the regression of Equation 9 to the abovementioned 10 min average concentration data.

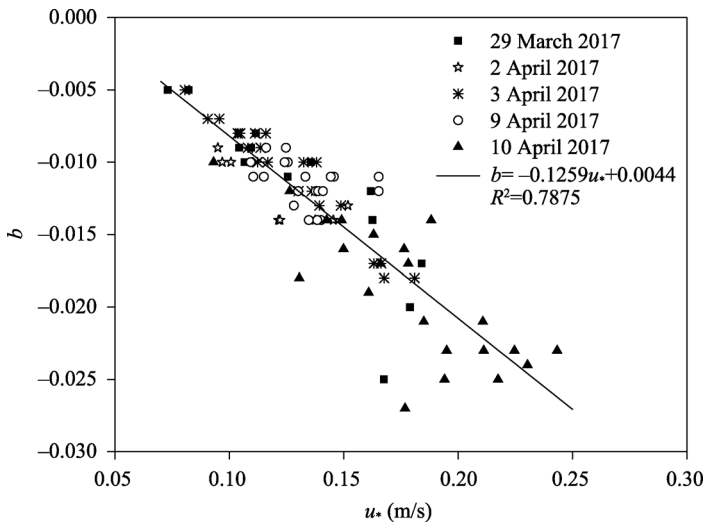

Fig. 3 Relationship between regression coefficient (b) for the profile in Equation 9 and friction velocity (u_*)

A linear correlation between b and u_* is shown in Figure 3, which is consistent with field observation results from Gillies and Berkofsky (2004). Thus, Equation 9 can be further expressed as follows:

$$\begin{cases} c(z) = b(u_*) \ln z + c(1) \\ b(u_*) = \mathrm{p} u_* + \mathrm{f} \end{cases} \quad u_{*pt} < u_* < u_{*t}, \tag{10}$$

where $b(u_*)$ is the linear function of the u_*; and p and f are the empirical parameters with the values of –0.1259 and 0.0044 in this study, respectively, according to Figure 3. From Equation 10, we can estimate the vertical concentration profiles of suspensions near the surface if we measured

the $c(z)$ at 1.00 m height above the ground surface and the u_*. Moreover, due to the close link of the parameter b with the u_*, not with surface conditions, the linear function $b(u_*)$ is supposed to be useful in general over extended areas.

3.2 Vertical concentration profiles of PM10 with saltation

A wind erosion event occurred in the study area on 5 April 2017 at a persistent and steady northeasterly wind direction from 15:00 to the nighttime hours. The 240 min of observation started at 14:08, and the u_* reached a steady state and remained over the u_{*t} (u_{*t} in the site used for measurements was approximately 0.230 m/s) after approximately 60 min (Fig. 4a).

In the first 60 min, the u_* exhibited an overall increasing trend. Specifically, the u_* fluctuated significantly, and the maximum instantaneous u_* exceeded the u_{*t}, but no continuous and obvious sand flow occurred above the ground surface. At this point, the significant fluctuation in PM10 concentrations at heights of 0.10 and 0.50 m was mainly caused by the aerodynamic lifting of loose dust particles on the surface (Fig. 4b and c). From 60 to 180 min, the u_* experienced a slight increasing trend, and the sand transport was active (Fig. 4d); nonetheless, PM10 concentrations at heights of 0.10 and 0.50 m decreased slightly with the increasing u_* before a slight increase but fluctuated significantly. After 180 min, the u_* steadily fluctuated, and the sand transport gradually weakened before ceasing altogether. During this period, PM10 concentrations at heights of 0.10 and 0.50 m gradually decreased to stable values but were not zero. PM10 concentrations at heights of 1.00 and 2.00 m were relatively stable throughout the observation period, and it was difficult to directly find their links with the u_* or sand flux (Fig. 4e and f).

Figure 4 shows that when the sand transport occurred, PM10 concentrations were greatly affected in the lower layer (heights of 0.10–0.50 m). PM10 concentrations significantly fluctuated and did not show obvious regularity, making it impossible to use a single logarithmic function to describe the vertical concentration profiles of PM10 suspensions during wind erosion periods. In the upper layer (heights of 1.00 and 2.00 m), PM10 concentrations did not change much and were little affected by the sand transport. In an earlier field study, Gillies and Berkofsky (2004) found that the logarithmic function could still be used to express the vertical concentration profiles of suspensions above the saltation layer (i.e., heights of 1.70–9.00 m in their study). Such evidence suggests that the vertical concentration profiles of PM10 suspensions above the saltation-affected layer are not directly affected by dust emissions during erosion periods under similar transport conditions to that without saltation; namely, it is still solely controlled by the wind conditions. Equation 10 was used to describe the vertical profile of the u_* in this study, which was further verified using the 10 min average suspension concentrations above the saltation-affected layer (heights of 1.00 and 2.00 m) (Fig. 5).

In other words, Equation 10 can well describe the vertical concentration profiles of PM10 suspensions above the saltation-affected layer during aeolian processes.

The above analysis confirmed that first, the heights of 0.10 and 0.50 m were in the saltation-affected layer, where the concentration of PM10 was greatly affected by saltation, whereas the heights of 1.00 and 2.00 m were beyond the saltation-affected layer, where the concentration of PM10 was determined by airflow transport. Second, there was a concentration transition height (TSA) between the saltation-affected layer and airflow-transport layer: the layer above the TSA was closely related to wind conditions, and Equation 9 can be used to express the relative concentration profile of PM10. Although PM10 concentration in the saltation-affected layer below the TSA was directly influenced by local dust emissions, there was no confirm conclusion on its relative concentration profile. The exponential function (Fryrear and Saleh, 1993), the power function (Nickling, 1978; Vories and Fryrear, 1991) and the logarithmic function (Leys and Mctainsh, 1996) have been used to express PM10 vertical concentration profiles in the saltation-affected layer in previous studies. In this study, we selected the exponential function. Then, the vertical concentration profile of PM10 suspensions is expressed in a piecewise manner as follows:

$$\begin{cases} c(z) = me^{nz} & z < \text{TSA} \\ c(z) = b\ln(z) + c(1) & z \geq \text{TSA} \end{cases} u_* > u_{*t}, \tag{11}$$

where m and n are the regression coefficients.

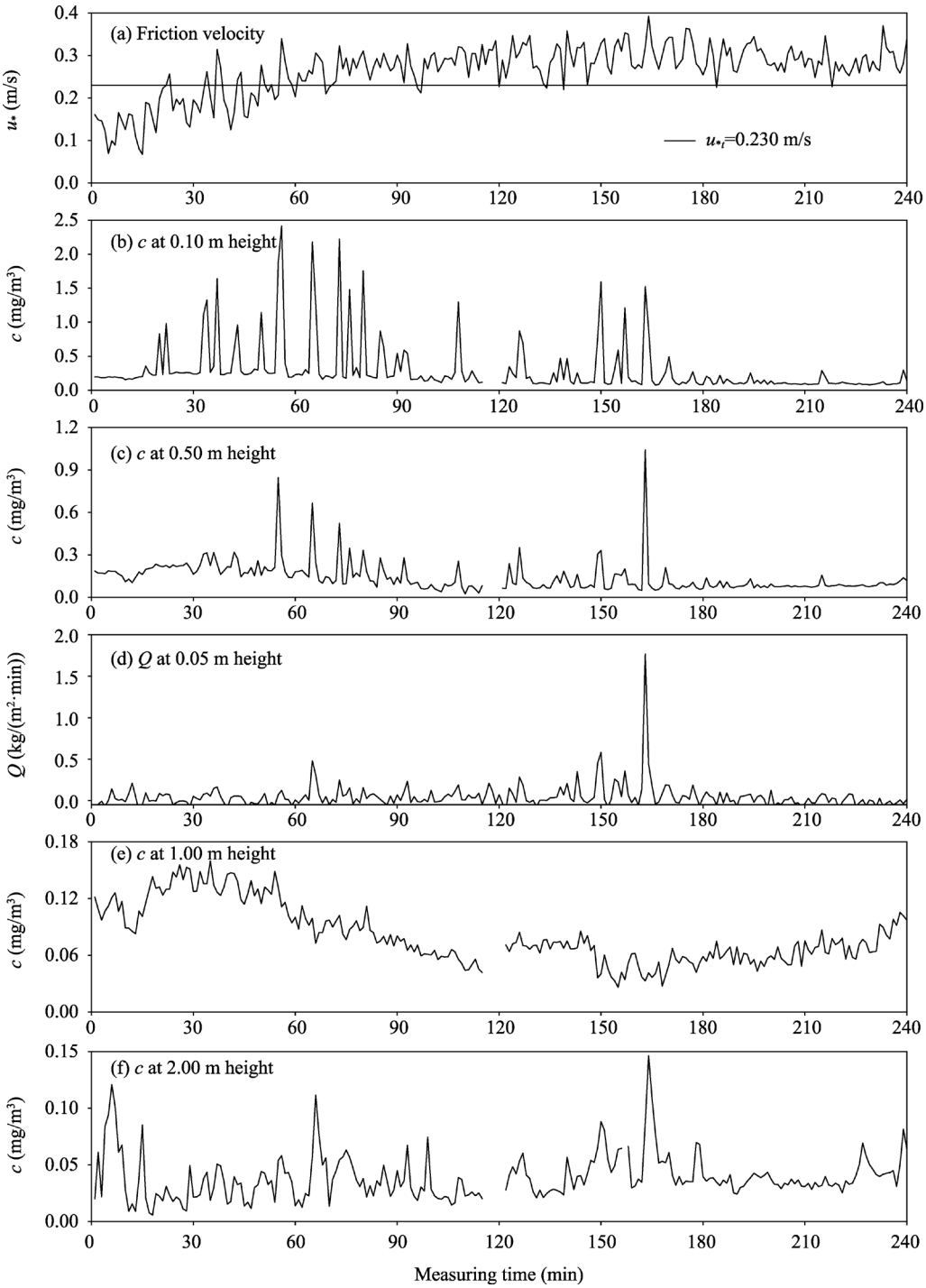

Fig. 4 Observations of the u_* (a), PM10 concentration (c) values at heights of 0.10, 0.50, 1.00 and 2.00 m (b, c, e and f, respectively), and sand flux (Q) at 0.05 m height (d) during wind erosion event between 14:08 and 18:08 (LST) on 5 April 2017. All values were 1 min averages, and PM10 concentration data between 16:03–16:08 were missing.

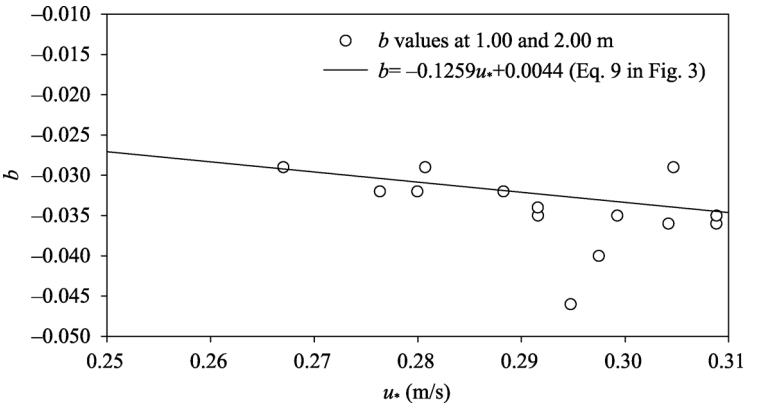

Fig. 5 Verification of the vertical profile of the u_* using the 10 min average suspension concentrations above the saltation-affected layer (heights of 1.00 and 2.00 m). b is the regression coefficient.

Since we confirmed that the heights of 0.10 and 0.50 m are in the saltation-affected layer and the heights of 1.00 and 2.00 m are in the TSA, we obtained the regression coefficients in Equation 11 by fitting $c(z)=me^{nz}$ with every 10 min average PM10 concentration at heights of 0.10 and 0.50 m and $c(z)=b\ln(z)+c(1)$ with every 10 min average suspension concentration at heights of 1.00 and 2.00 m. Then, the height of intersection point between the two functions should be the TSA. Table 1 shows the results and the corresponding observation data from 91 to 240 min. In the period of 91–140 min, the TSA fluctuated approximately 0.60 m. From 141 to 170 min, the TSA increased to a maximum of 0.77 m. Because PM10 concentration data at the three upper heights can be expressed as a logarithmic function, the TSA was less than 0.50 m from 171 to 240 min. According to Table 1, there was a strong correlation between the u_* and TSA from 91 to 170 min (r=0.70, P<0.001), while this was not the case after 171 min. This suggests that the u_* is not vital in affecting the TSA. Therefore, the TSA is only related to the u_* under certain conditions. This agreed with the consensus that the saltation of soil particles and aggregates during aeolian processes is the most crucial physical mechanism of dust emissions. In addition, the TSA indicated the upper limit influence of local dust emissions. Its value directly reflected dust emission intensity. During wind erosion, the trend in dust emission intensity was generally from weak to strong and then weakened until dust emissions almost ceased, as shown in the TSA column in Table 1.

4 Discussion

4.1 Dust emission rate (f_v) during wind erosion

The key issue as well as the most practical problem associated with wind erosion are the rate and quantity of soil loss (Kok et al., 2012). For short-distance movement (i.e., saltation and "creep") of large particles during wind erosion, both surface erosion and deposition occur simultaneously. Thus, soil loss by wind transport should be equal to the difference between erosion quantity and deposition quantity (Shao, 2008). For suspensions, once small dust particles are blown off the surface, deposition can be negligible. Therefore, the quantity of dust emissions equals the dust loss by wind erosion. In contrast, the study of dust loss during erosion processes is more feasible and convincing than that of soil transport in saltation and creep.

Currently, two main model designs are used to estimate dust emissions caused by wind erosion. One is based on microscopic mechanisms of emission processes represented by the dust production model (Alfaro et al., 2001; Shao, 2008; Kok et al., 2012). This model design has a set of sophisticated parameters for surface features (e.g., soil texture, moisture, etc.) as well as physical mechanisms. Due to the complexity of natural conditions compared to those in wind tunnels, this model design is now more applicable to the theoretical estimation of dust emissions

Table 1 Parameters associated with dust emissions during the wind erosion event on 5 April 2017

Time (min)	Saltation		Suspension		TSA (m)	u_* (m/s)
	m	n	b	$c(1)$		
91–100	0.282	–2.195	–0.033	0.061	0.58	0.267
101–110	0.322	–2.176	–0.029	0.064	0.66	0.295
111–120	0.408	–3.064	–0.037	0.052	0.56	0.292
121–130	0.288	–1.872	–0.042	0.071	0.61	0.304
131–140	0.232	–1.610	–0.032	0.070	0.62	0.280
141–150	0.430	–2.359	–0.040	0.072	0.67	0.297
151–160	0.376	–2.381	–0.036	0.058	0.70	0.309
161–170	0.463	–1.882	–0.040	0.098	0.77	0.312
171–180	-	-	–0.029	0.058	<0.50	0.305
181–190	-	-	–0.034	0.061	<0.50	0.292
191–200	-	-	–0.035	0.059	<0.50	0.309
201–210	-	-	–0.032	0.057	<0.50	0.288
211–220	-	-	–0.029	0.062	<0.50	0.281
221–230	-	-	–0.032	0.067	<0.50	0.276
231–240	-	-	–0.035	0.090	<0.50	0.299

Note: m, n, b and $c(1)$ represent regression coefficients in Equation 11; TSA is the concentration transition height between the saltation-affected layer and airflow-transport layer; u_* is the friction velocity. -, no data.

for both expansive areas and large timescales. It, however, does not provide an accurate description of dynamic changes in dust emissions during aeolian processes in the field. The other model design is based on turbulent and molecular diffusion and by analogy to scalar fluxes represented by Gillette (1978), which is simple and is used more often in wind tunnels and field experiments (Shao, 2008). However, in the actual use of this model, the vertical concentration profile is generally simplified as a single linear form attained from concentrations measured at two certain heights, by ignoring the influence of dust emission on the profile (i.e., below the TSA) during wind erosion.

Among the three widely accepted mechanisms of dust emissions, when compared to the ejection of dust aerosols from soil aggregates by impacting saltating particles and the ejection of dust aerosols from soil aggregates that disintegrate during saltation processes, direct aerodynamic lifting is a substantially less important source of dust aerosols (Gillette et al., 1974; Loosmore and Hunt, 2000; Kok et al., 2012). Moreover, this latter source typically occurs at the beginning of wind speed rise and is greatly restricted to the supply of wind-erodible sediment (Sweeney et al., 2008; Wu et al., 2018). Thus, dust emissions caused by direct aerodynamic lifting have little influence on near-surface suspended PM10 concentrations during aeolian processes (Shao, 2008; Kok et al., 2012). Under ideal conditions, suspensions above the TSA are all composed of suspended PM10 particles transported from upwind directions, and suspensions below the TSA are composed of PM10 particles emitted by both local and upwind areas.

Therefore, the local f_v is equal to the difference between the horizontal total suspension transport rate and the suspension transported from upwind directions (Shao, 2008). Assuming that the vertical concentration profile of suspensions transported from upwind directions below the TSA is not affected by sand saltation and local dust emissions, we can still use Equation 10 to describe the vertical concentration profile of the outside aeolian suspensions in the saltation-affected layer. Therefore, the f_v (mg/(m•s)) can be expressed as the difference between the total horizontal suspension transport rate (q_d; mg/(m•s)) and the horizontal suspension (q_{d0}; mg/(m•s)) transported from upwind directions in the saltation-affected layer:

$$f_v = q_d - q_{d0} = \int_{z_0}^{\mathrm{TSA}} c(z)u(z)\mathrm{d}z - \int_{z_0}^{\mathrm{TSA}} c'(z)u(z)\mathrm{d}z = \int_{z_0}^{\mathrm{TSA}} me^{nz}u(z)\mathrm{d}z - \int_{z_0}^{\mathrm{TSA}} (b\ln z + c(1))u(z)\mathrm{d}z \quad (12)$$

where $c'(z)$ (mg/m^3) is the concentration of suspensions transported from upwind directions at z height below the TSA, which can be deduced from $c(z)$ above the TSA and is expressed by Equation 10. Parameters of b and $c(1)$ were acquired by fitting the measured suspension concentrations above the TSA, and m and n were acquired from the fitting below the TSA. The f_v from 91 to 140 min and from 141 to 170 min calculated using Equation 12 were 0.238 and 0.440 mg/(m•s), respectively. After 170 min, the f_v decreased to almost zero. Therefore, the dust lost (i.e., the quantity of loss through dust emissions) in the study site during a 180 min wind erosion event calculated using Equation 7 was approximately 1.44 g/m.

This computational method of the f_v based on changes in dust emissions during wind erosion truly links the horizontal suspension transport to the vertical dust emissions. Compared to previous methods (Nickling and Gillies, 1993; López, 1998; Zobeck and Pelt, 2006; Wagenbrenner et al., 2013; Wang and Zhang, 2021), the computational method showed the influence of saltation intensity on dust emissions through the TSA and regression coefficients in Equation 11. Above all, this method can be used to separate local dust emissions from aeolian suspension from upwind sources, so that dynamic changes in local dust emissions and aeolian suspension transport can be quantitatively expressed.

4.2 Influence of surface renewal on dust emissions

Currently, dust emission models are generally transport-limited; namely, emissions are solely governed by wind forces. However, natural arid environments are dominated by supply-limited surfaces, which means that emissions are controlled by the availability of erodible grains (Macpherson et al., 2008; Shao, 2008; Zhang et al., 2016; Zhang et al., 2022). Therefore, the practicality of such models is significantly limited, and determining mechanisms that limit surface dust is the key to solving this problem. In Section 3.2, it was shown that saltation intensity and dust emissions were significantly correlated to the u_* in the first 170 min of the wind erosion event, while saltation intensity and the f_v decreased significantly after 170 min even though the u_* did not significantly decrease. In Table 2, we compared the soil texture in the 0–1 cm soil layer at height of 2.00 m upwind from the measuring site before and after the erosion event. The results showed that particles finer than 10 μm in the surface sediments decreased after the wind erosion event; however, there was still a considerable amount supplying dust emissions.

Table 2 Particle size composition of the surface sediments before and after the erosion event on 5 April 2017

Erosion event	Particle size composition (%)						Mean particle size (μm)
	<2 μm	2–63 μm	63–250 μm	250–500 μm	500–2000 μm	>2000 μm	
Before the erosion event	1.9	13.3	48.0	5.2	11.2	20.6	708.1
After the erosion event	1.4	12.2	45.6	4.1	20.8	15.8	709.6

Moreover, the proportion of coarse sand significantly increased, and the coarsening of the surface soil texture was obvious. The reason for decreasing dust emissions after 170 min is the gradual limitation of the supply of erodible grains as a result of surface renewal with erosion progresses, which will change the surface transition type from limited transportation to limited supply. Under this level of the u_*, soil texture coarsening forms a protective layer over erodible particles that acts against the corresponding u_* by weakening saltation and dust emissions. It is clear that if the subsequent u_* increases to a degree that allows the shear force against the surface to exceed such protection, saltation processes and dust emissions will continue, and this trend will continue to occur from 90 to 240 min. Such evidence suggests that the surface supply of erodible grains is the determining factor for saltation intensity. When there is a sufficient supply of

erodible grains, there will be a significant correlation among the u_*, saltation intensity and f_v. When the supply is limited by factors such as surface renewal or an increase in soil moisture, the u_* will not necessarily be associated with the former two. Although this study did not consider further issues related to the relationship between saltation intensity and f_v, we plan to investigate abrasion efficiency (the ratio of the f_v to saltation flux) in aeolian processes in a future study.

In arid regions, sustained high wind speeds on the ground surface do not reach the point of suspensions, where there would be no dust supply. A known property is that when surface renewal occurs as erosion progresses, surface soil texture coarsening will reach a point where a protective layer of erodible particles forms at a corresponding u_*; then sand transport and dust emissions will cease (Zhang et al., 2016; Wang et al., 2021). Therefore, future soil loss models designed for both saltation particles and dust emissions should be based on all wind erosion events, and dynamic changes in various parameters during aeolian processes should also be taken into consideration, especially detailed responses of surface soil texture and erodible grain supplies to relative wind speeds at all levels as well as their overall duration (Zhang et al., 2018). Although the results from our field investigation are much simpler than those found in actual environments, this is typical of dust emission processes on the Gobi surface during aeolian processes.

From the calculation of the results in Section 3.1, we found that during the most intense period of wind erosion (i.e., 90–170 min), the f_v accounted for only approximately a quarter of the total horizontal suspension transport rate below the TSA. After 170 min, the horizontal transport rate of suspended particles introduced from upwind directions accounted for nearly 100.0%. For near-surface suspension concentrations during wind erosion, contributions from other sources of suspended transport were much greater than local dust emissions. Therefore, the contribution of the Gobi surface to atmospheric dust was limited (Wang and Zhang, 2021; Zhang et al., 2022). Moreover, observed suspended particles transported from upwind directions were mainly derived from the erodible surface around the Gobi desert and its interior (e.g., sand dunes, playa, alluvial fans, etc.). However, the observed results would be different when the upwind surface and local surface conditions change. For instance, if the upwind surface has a lower dust emission ability than the local surface, the local dust emissions would be higher than the upwind suspension. Additionally, the gravel coverage of the local surface has significant effects on the calculation results (Wang and Zhang, 2021; Zhang et al., 2022). Therefore, if the gravel coverage of the local surface is higher than the present, the dust emission constitutes a smaller proportion of the total horizontal suspension. Therefore, extra observations on other kinds of surface conditions should be carried out further. This paper proposed a method that can separate dust emissions from the total suspension in airflow regardless of the upwind surface and local surface conditions.

5 Conclusions

This study analyzed measured data of wind profiles, PM10 concentrations at different heights and sand transport on a Gobi surface. On the Gobi surface with a sufficient supply of dust, the vertical concentration profiles of PM10 matched the logarithmic model without aeolian saltation better ($u_{*pt}<u_*<u_{*t}$). For aeolian processes with saltation ($u_*>u_{*t}$), we divided the profile into the saltation-affected layer and the airflow-transport layer according to the two different sources of suspensions (i.e., locally emitted dust and upwind transported dust). The profile was expressed in a piecewise manner with the TSA as the boundary between the saltation-affected layer and the airflow-transport layer. Based on the vertical concentration profiles, we used a mathematical method to separate emitted dust from total suspension in airflow and proposed a computational method from a new perspective to calculate the f_v to directly describe changes in dust emissions during aeolian processes. The calculated dust loss on the Gobi surface during a 180 min wind erosion event was approximately 1.44 g/m. In the present study, only one kind of surface condition was studied. In the future, extra observations on the other kinds of surface conditions are recommended.

Acknowledgements

This work was supported by the National Natural Science Foundation of China (41630747).

References

Alfaro S C, Gomes L. 2001. Modeling mineral aerosol production by wind erosion: Emission intensities and aerosol size distributions in source areas. Journal of Geophysical Research: Atmospheres, 106(D16): 18075–18084.

Anderson R S, Hallet B. 1986. Sediment transport by wind: Toward a general model. Geological Society of America Bulletin, 97(5): 523–535.

Bagnold R A. 1941. The Physics of Blown Sand and Desert Dunes. Dordrecht: Springer, 1–265.

Budd W F. 1965. The drifting of non-uniform snow particles. Studies in Antarctic Meteorology, 9: 59–70.

Dong Z B, Man D Q, Luo W Y, et al. 2010. Horizontal aeolian sediment flux in the Minqin area, a major source of Chinese dust storms. Geomorphology, 116(1): 58–66.

Freire L S, Chamecki M, Gillies J A. 2016. Flux-profile relationship for dust concentration in the stratified atmospheric surface layer. Boundary-Layer Meteorology, 160(2): 249–267.

Fryrear D W, Saleh A. 1993. Field wind erosion: vertical distribution. Soil Science, 155(4): 294–300.

Gillette D A. 1974. On the production of soil wind erosion having the potential for long range transport. Journal of Geophysical Research Atmospheres, 8: 734–744.

Gillette D A, Walker T R. 1977. Characteristics of airborne particles produced by wind erosion of sandy soil, high plains of West Texas. Soil Science, 123(2): 97–110.

Gillette D A. 1978. A wind tunnel simulation of the erosion of soil: Effect of soil texture, sandblasting, wind speed, and soil consolidation on dust production. Atmospheric Environment, 12(8): 1735–1743.

Gillette D A, Fryrear D W, Gill T E, et al. 1997. Relation of vertical flux of particles smaller than 10 μm to total aeolian horizontal mass flux at Owens Lake. Journal of Geophysical Research: Atmospheres, 102(D22): 26009–26015.

Gillies J A, Berkofsky L. 2004. Eolian suspension above the saltation layer, the concentration profile. Journal of Sedimentary Research, 74(2): 176–183.

Hagen L J, Van Pelt S, Sharratt B. 2010. Estimating the saltation and suspension components from field wind erosion. Aeolian Research, 1(3): 147–153.

Hinds W C. 2000. Aerosol technology: Properties, behavior, and measurement of airborne particles. New York: John Wiley & Sons, 1121–1122.

Houser C A, Nickling W G. 2001. The emission and vertical flux of particulate matter <10 μm from a disturbed clay-crusted surface. Sedimentology, 48(2): 255–267.

Kind R J. 1992. One-dimensional aeolian suspension above beds of loose particles: a new concentration profile equation. Atmospheric Environment, 26(5): 927–931.

Kjelgaard J, Sharratt B, Sundram I, et al. 2004. PM10 emission from agricultural soils on the Columbia Plateau: comparison of dynamic and time-integrated field-scale measurements and entrainment mechanisms. Agricultural and Forest Meteorology, 125(3–4): 259–277.

Kok J F, Parteli E J R, Michaels T I, et al. 2012. The physics of wind-blown sand and dust. Reports on Progress in Physics, 75(10): 10690, doi: 10.1016/j.aeolia.2015.02.003.

Leys J F, Mctainsh G H. 1996. Sediment fluxes and particle grain-size characteristics of wind-eroded sediments in southeastern Australia. Earth Surface Processes and Landforms, 21(7): 661–671.

Loosmore G A, Hunt J R. 2000. Dust resuspension without saltation. Journal of Geophysical Research: Atmospheres, 105(D16): 20663–20671.

López M V. 1998. Wind erosion in agricultural soils: an example of limited supply of particles available for erosion. CATENA, 33(1): 17–28.

Macpherson T, Nickling W G, Gillies J A, et al. 2008. Dust emissions from undisturbed and disturbed supply-limited desert surfaces. Journal of Geophysical Research, 113(F2), doi: 10.1029/2007JF000800.

Nickling W G. 1978. Eolian sediment transport during dust storms: Slims River Valley, Yukon Territory. Canadian Journal of Earth Sciences, 15(7): 1069–1084.

Nickling W G, Gillies J A. 1993. Dust emission and transport in Mali, West Africa. Sedimentology, 40(5): 859–868.

Prandtl L. 1953. Essentials of Fluid Dynamics with Applications to Hydraulics, Aeronautics, Meteorology and other Subjects. London: Blackie & Son, 1–99.

Pye K, Tsoar H. 2009. Aeolian Sand and Sand Dunes. Berlin: Springer, 1–106.

Qiu X F, Zeng Y, Miao Q L. 2001. Temporal-spatial distribution as well as tracks and source areas of sand-dust storms in China. Acta Geographica Sinica, 56(3): 316–322.

Shao Y P, Lu H. 2000. A simple expression for wind erosion threshold friction velocity. Journal of Geophysical Research, 105(D17): 22437–22443.

Shao Y P. 2008. Physics and Modelling of Wind Erosion. Heidelberg: Springer, 1–278.

Shao Y P, Wyrwoll K, Chappell A, et al. 2011. Dust cycle: An emerging core theme in Earth system science. Aeolian Research, 2(4): 181–204.

Shao Y P, Zhang J, Ishizuka M, et al. 2020. Dependency of particle size distribution at dust emission on friction velocity and atmospheric boundary-layer stability. Atmospheric Chemistry and Physics, 20: 12939–12953.

Sharratt B, Pi H. 2018. Field and laboratory comparison of PM10 instruments in high winds. Aeolian Research, 32: 42–52.

Sweeney M, Etyemezian V, Macpherson T, et al. 2008. Comparison of PI-SWERL with dust emission measurements from a straight-line field wind tunnel. Journal of Geophysical Research: Atmospheres, 113(F1): 228–236.

Vories E D, Fryrear D W. 1991. Vertical distribution of wind-eroded soil over a smooth, bare field. Transactions of the Asae, 34(4): 1763–1768.

Wagenbrenner N S, Germino M J, Lamb B K, et al. 2013. Wind erosion from a sagebrush steppe burned by wildfire: Measurements of PM10 and total horizontal sediment flux. Aeolian Research, 10: 25–36.

Wang R D, Li Q, Zhou N, et al. 2019. Effect of wind speed on aggregate size distribution of windblown sediment. Aeolian Research, 36: 1–8.

Wang R D, Li Q, Wang R J, et al. 2021. Influence of wind velocity and soil size distribution on emitted dust size distribution: A wind tunnel study. Journal of Geophysical Research: Atmospheres, 126, e2020JD033768, doi: doi.org/10.1029/2020JD033768.

Wang X S, Zhang, C L. 2021. Field observations of sand flux and dust emission above a gobi desert surface. Journal of Soils and Sediments, 21: 1815–1825.

Wang X S, Zhang C L, Zou X Y. 2021. A model of the sand transport rate that accounts for temporal evolution of the bed. Geomorphology, 378, 107616, doi: 10.1016/j.geomorph.2021.107616.

Whicker J, Breshears D D, Field J P. 2014. Progress on relationships between horizontal and vertical dust flux: Mathematical, empirical and risk-based perspectives. Aeolian Research, 14: 105–111.

Wu W, Yan P, Wang Y, et al. 2018. Wind tunnel experiments on dust emissions from different landform types. Journal of Arid Land, 10(4): 1–13.

Zender C S, Bian H, Newman D. 2003. Mineral Dust Entrainment and Deposition (DEAD) model: Description and 1990s dust climatology. Journal of Geophysical Research, 108(D14): 4416, doi: 10.1029/2002JD002775.

Zhang C L, Song C Q, Wang Z T, et al. 2018. Review and prospect of the study on soil wind erosion process. Advances in Earth Science, 33(1): 27–41. (in Chinese)

Zhang C L, Wei G R, Zou X Y, et al. 2022. The varying fetch effect of aeolian sand transport above a gobi surface and its implication for gobi development process. International Soil and Water Conservation Research, doi: 10.1016/j.iswcr.2022.03.002.

Zhang J, Teng Z J, Huang N, et al. 2016. Surface renewal as a significant mechanism for dust emission. Atmospheric Chemistry and Physics, 16(24): 15517–15528.

Zhang Y Y, Hu R F, Zheng X J. 2018. Large-scale coherent structures of suspended dust concentration in the neutral atmospheric surface layer: A large-eddy simulation study. Physics of Fluids, 30(4): 046601, doi: 10.1063/1.5022089.

Zobeck T M, Pelt R. 2006. Wind-induced dust generation and transport mechanics on a bare agricultural field. Journal of Hazardous Materials, 132(1): 26–38.